Influence of carbon nanotubes on printing quality and mechanical properties of 3D printed cementitious materials

Ali, Mohd Mukarram; Nassrullah, Ghaith; Abu Al-Rub, Rashid K.; El-Khasawneh, Bashar; Ghaffar, Seyed Hamidreza; Kim, Tae Yeon

DOI:
10.1016/j.dibe.2024.100415

Developments in the Built Environment 18 (2024) 100415

Contents lists available at ScienceDirect

Developments in the Built Environment

journal homepage: www.sciencedirect.com/journal/developments-in-the-built-environment

Influence of carbon nanotubes on printing quality and mechanical properties of 3D printed cementitious materials

Mohd Mukarram Ali [a,b], Ghaith Nassrullah [a], Rashid K. Abu Al-Rub [b], Bashar El-Khasawneh [b], Seyed Hamidreza Ghaffar [c,d], Tae-Yeon Kim [a,b,*]

[a] Civil and Environmental Engineering, Khalifa University of Science and Technology, Abu Dhabi, 127788, United Arab Emirates
[b] Advanced Digital & Additive Manufacturing Centre, Khalifa University of Science and Technology, Abu Dhabi, 127788, United Arab Emirates
[c] Civil Engineering, University of Birmingham, Dubai International Academic City, Dubai, P.O. Box 341799, United Arab Emirates
[d] Applied Science Research Center, Applied Science Private University, Amman, 11937, Jordan

ARTICLE INFO

Keywords:
Additive manufacturing
Optimal mix design
Printability
Carbon nanotubes
Compressive strength
Flexural strength
Nanoscale bridges

ABSTRACT

This paper presents the impact of incorporating carbon nanotubes (CNTs) into the 3D printing of cementitious materials, along with the effective dispersion of CNTs. Compared to the control mix, adding CNTs with superplasticizer significantly enhanced the printing quality by reducing the error in height of two-layers from 38% to 30% and an 81% enhancement in the buildability. Moreover, rheology properties revealed shear-thinning behaviour with lower viscosity, resulting in improved flowability. The progressive increase in CNT concentrations up to 0.2% yielded a noteworthy improvement in the mechanical properties. At 28 days, the incorporation of 0.2% CNTs resulted in a significant increase in the flexural strength, compressive strength, and Young's modulus by 99%, 72%, and 43%, respectively, compared to the mix containing silica fume. Microstructural investigation of the CNT-cement matrix revealed nanoscale crack bridges formed by CNTs, reinforcing the cementitious material and improving its mechanical properties.

1. Introduction

Additive Manufacturing (AM) also known as 3D printing is an innovative technology, evolved from the layer-by-layer fabrication of three-dimensional (3D) structures directly from computer-aided design (CAD) drawings (Wu et al., 2016). 3D printing technology has emerged as a significant digital fabrication technique in the construction industry because of its advantages over traditional casting, such as lower waste, lower cost, more architectural flexibility with intricate geometries, improved mechanical properties, and faster construction (Buswell et al., 2020; Baduge et al., 2021; Asprone et al., 2018; Khan et al., 2024). For large-scale construction, two types of printers, robotic arm printing and gantry concrete printing are frequently used in the process of concrete 3D printing. Due to its simplicity, the gantry is typically better suited for large-scale printing. However, the robotic printer is more practically appropriate for printing complex objects due to its 6-axis rotational capability (Puzatova et al., 2023; Paolini et al., 2019). The two primary categories of cement 3D printing methods are powder printing and extrusion printing. Powder-based printing, involves the layer-by-layer application of a liquid binder by a print head to a cement-based substrate. In extrusion-based manufacturing, a cementitious material is extruded in a layer-by-layer form from a nozzle in an automated system. Extrusion-based method makes construction easier in larger spaces, while powder bed methods offer more design freedom and higher accuracy (Panda et al., 2023; Sanjayan et al., 2018).

In the present study, an extrusion-based method was used in which cement mortar was extruded with a newly fabricated extruder and nozzle. In this method, implementing 3D printing with cementitious materials poses certain challenges, involving a careful balance of printability, buildability, and the rheology of the mixture. It often exhibits significant irregularities in their pores and voids relative to conventional methods (Pasupathy et al., 2022). This can be attributed to factors such as movement of the print head, absence of vibration, compaction, and quick moisture loss caused by the large surface area (Casagrande et al., 2022). Moreover, the shape and size of nozzle in extrusion-based technique have a considerable impact on printing quality and the buildability of the printed products, which is critical for a successful print (Bikas et al., 2016). Shakor et al. (2019) studied the

* Corresponding author. Civil and Environmental Engineering, Khalifa University of Science and Technology, Abu Dhabi, 127788, United Arab Emirates
E-mail address: taeyeon.kim@ku.ac.ae (T.-Y. Kim).

https://doi.org/10.1016/j.dibe.2024.100415
Received 25 January 2024; Received in revised form 6 March 2024; Accepted 22 March 2024
Available online 25 March 2024

effect of different nozzle shapes and demonstrated that the use of a caulking gun in conjunction with a 6-degree-of-freedom robot printer resulted in fiber-reinforced mortar with enhanced mechanical strength. Furthermore, the layer-by-layer deposition process might result in variations in printing quality, leading to the formation of weaker bonds between the layers, potentially effecting the mechanical properties of cement-based structures. Most importantly, incorporating nanomaterials into 3D printed cementitious materials are expected to minimize the setting time, limit pores and voids, reduce drying shrinkage, improve printing quality, and enhance the mechanical properties of cementitious materials (Cui et al., 2022). Among the various nanomaterials, carbon nanotubes (CNTs) were used in this study to investigate their impact on 3D printed cementitious materials. CNTs have garnered significant attention in the field of materials science due to their remarkable characteristics. CNTs are cylindrical nanostructures, comprised of carbon atoms arranged in a hexagonal pattern. They exhibit exceptional properties such as high mechanical strength, resistance to oxidation and corrosion, high conductivity, and thermal properties (Abubakre et al., 2023; Arash et al., 2014; Li and Li, 2022; Fang et al., 2021; Balaji et al., 2024). The primary area of investigation on CNTs in construction has centered around their incorporation into cement-based materials to create nanocomposites with enhanced mechanical properties, such as increased compressive and flexural strengths, as well as higher durability (Sheikh et al., 2021; Zhang et al., 2023).

Earlier studies revealed that adding CNTs to cementitious materials provides exceptional strengthening as well as crack control (Ramezani et al., 2022). Abu Al-Rub et al. (Abu Al-Rub et al., 2012a) investigated the effects of adding both short and long multi-walled carbon nanotubes (MWCNTs) to cement paste at varying concentrations (mainly 0.1% and 0.2%). Three-point bending tests demonstrated notable improvements in flexural strength, i.e., a 269% increase for short 0.2% MWCNTs and a 65% increase for long 0.1% MWCNTs at 28 days. Abu Al-Rub et al. (Abu Al-Rub et al., 2012b) also studied the impact of CNTs by comparing the performance of treated and untreated nano-filaments in the cement paste. After 28 days, cement paste treated with CNTs showed significant increases, including an average of 73% greater ductility, 60% higher flexural strength, 25% enhancement of Young's modulus, and a remarkable 170% higher modulus of toughness than plain cement.

Previous efforts to improve the performance of 3D printable cementitious composites via the inclusion of nano-additives like attapulgite nano-clay, nano-graphite platelets, and natural and calcined halloysite clay minerals have been reported with some encouraging results (Chougan et al., 2020, 2021, 2022; Sikora et al., 2021). On the other hand, Shakor et al. (2020) demonstrated that the inclusion of E6-glass fibers as reinforcement in 3D printing of cement mortar, along with heat-curing, enhances the mechanical properties and surface quality of printed samples. Heat-curing at an optimal temperature of 80 °C achieved the highest compressive strength. However, there are few investigations on incorporating CNTs into 3D printing of cement-based materials. For example, Sun et al. (2020) studied the effect of MWCNTs in 3D-printed polyvinyl alcohol (PVA) mortar ink, ranging from 0.01 to 0.1% weight of cement. This study did not use dispersion techniques to mix or disperse MWCNTs in water. It was found that the addition of MWCNTs in small amounts had no effect on workability and buildability, but did reduce flowability by 3.7% for 0.1% MWCNTs when compared to the control sample. Notably, the optimum concentration of 0.1% MWCNTs resulted in a 33.6% increase in compressive strength at 3 days, while 0.05% MWCNTs improved flexural strength by 46%. However, the compressive and flexural strengths at 28 days remained constant. Kan et al. (2022) examined the effects of incorporating 0.05% of MWCNTs into cementitious material for the purpose of 3D printing. MWCNTs were mixed in an aqueous solution using a magnetic agitator device as a dispersion technique. The workability of the mixture remained unchanged; however, there was an improvement in its mechanical properties, resulting in a shift from brittle to ductile failure due to a reduction in the porosity of the printed material by a volume of 0.01 mm^3. Wang et al. (Wang and Aslani, 2023) studied 3D printed self-sensing cementitious composites by adding 0.05% CNTs and 0.3% carbon fibers (CFs), both by percentage weight of cement, to the basic mix. The mechanical mixer was employed as the dispersion method for mixing the MWCNTs. In flexural loading experiments, reinforced concrete (RC) beams with 0.05% CNTs showed 10% higher average load capacity (88.65 kN) and 12% higher maximum load (111.09 kN) than controlled RC beams. The study found that adding CFs and CNTs to concrete beams enhanced strain ductility, reduced crack propagation, and minimized deformation. Dulaj et al. (2022) investigated the effects of MWCNTs at varying concentrations (0%, 0.05%, and 0.1% by weight of binder content) on 3D printed cementitious materials. Higher concentrations (specifically, 0.1% MWCNTs by weight of binder content) resulted in poor flowability and reduced mechanical properties, particularly compressive strength, because of mixing MWCNTs without sonication, leading to the formation of agglomeration within the cementitious material. Consequently, optimal mechanical performance was achieved with a 0.05% MWCNTs concentration.

Nevertheless, limited research has been done on incorporating CNTs into 3D printed cementitious materials, and a major knowledge gap exists in enhancing printing quality, buildability and mechanical properties through proper dispersion of CNTs and avoiding the formation of agglomeration within the cement matrix. To address this issue, this study focuses on enhancing printing quality, buildability, and mechanical properties by facilitating the sonication process for dispersion of CNTs at higher concentrations (specifically, 0.1% and 0.2% of the weight of cement).

In this study, a Delta WASP 3D printer designed for clay materials was modified with a newly fabricated extruder and an appropriately designed nozzle for 3D printing of cementitious materials. The optimal printable mix design for the modified 3D printer was determined for the control mix, composed of cement, sand, and water. Moreover, two different nozzle shapes, i.e., square and circular, were designed and fabricated, and their effects on printing quality and buildability were examined using the control mix. The optimal printable mix designs for the mixes, including CNTs and SF in the control mix, were determined. Surfactants such as sodium dodecyl-benzene sulfonate (SDBS) or superplasticizers were added to the CNTs' solution and subjected to sonication using a liquid processor ultrasonic wave mixer in order to have proper dispersion and flowability. The effect of CNTs on printing quality and buildability was then investigated by comparing quantitatively with the results from the control mix and the mix including SF. In addition, the rheology of the optimal printable mixes was assessed using a rheometer to gauge their viscosity and shear stress. Subsequently, compressive and flexural strength tests were carried out to evaluate the influence of CNTs on the mechanical properties of 3D printed cementitious materials by varying their concentrations (0-0.2%). The outcomes were then compared with a mix containing only SF. Furthermore, the microstructural analysis was performed using a scanning electron microscope (SEM) to meticulously examine both intact and fractured surfaces of the specimens to gain insights into the modifications in mechanical properties of the 3D printed cementitious materials resulting from the addition of CNTs.

2. Experimental setup

The experimental setup was divided into three sub-divisions mainly, 3D printer system, materials and CNTs preparation method, and testing protocols for various experiments. This structured approach offers clarity and coherence in describing the experimental framework.

2.1. 3D printer system

For 3D printing using cementitious materials, the Delta WASP 20x40 3D printer, originally designed for printing clay and plastic materials,

was utilized in conjunction with the newly built extruder designed for simple extrusion of cementitious materials. Fig. 1(a) illustrates the Delta WASP 3D printer along with extruder attached to six axes arm. The extruder as shown in Fig. 1(b) was developed based on knowledge of the rheology, workability, flowability, and extrudability of cementitious material mixes. The extruder design consists of a 400 g maximum capacity hopper for the mix, a 12 cm long screw with a 5 mm pitch for pushing the material through the nozzle, the nozzle shaping the material extrusion output, and a WASP motor to drive the screw as seen in Fig. 1 (c). Moreover, two different shapes of nozzles, i.e., circular and square, were designed for the extruder, as shown in Fig. 1(d) and (e). The circular nozzle has a diameter of 5 mm, whereas the square nozzle has sides of 5 mm with R-1, i.e., a radius of 1-inch bend at the corners. These nozzles are attached to the extruder and connected to the WASP printer.

2.2. Materials and dispersion of CNTs

A convenient cementitious material is a mixture of cement, water, sand, chemical admixtures, additives, and fibers. Type I Ordinary Portland cement (CEM-1 42.5 N) was used as a cement. The extremely fine sand with particle sizes less than 0.30 mm, based on the ASTM E11 #50 sieve analysis, was used to avoid any blockage from large particles during the extrusion from a nozzle. As silica fume (SF), microsilica from Elkem, which was approved according to ASTM C 1240 (ASTM C 1240/C 1240M – 18, 2020), was employed. SF enables the rapid creation of a stable framework of extrudable mortar, which is suitable for 3D printing (Rubio et al., 2017). As a result, the layers sustain the load of the subsequent layers without failure. Master-Glenium ACE 456 from Master Builders BASF chemicals was used as a superplasticizer. In this study, the superplasticizer was also used as a surfactant to improve flowability and disperse CNTs in cement-based materials. CNTs used in this work were obtained from Applied Nanostructured Solutions, LLC (USA), a Lockheed Martin Corporation subsidiary. These CNTs were Polyethylene Glycol Functionalized (PEG) and classified as MWCNTs. CNTs were mainly used as a fiber to enhance the flexural, and compressive strengths of 3D printed cementitious materials. For proper dispersion of CNTs in water, sodium dodecyl-benzene sulfonate (SDBS) was also used as a surfactant. It plays a crucial role in reducing the surface tension between water and CNTs, thereby enhancing the dispersion of CNTs in water.

The uneven distribution of CNTs has an adverse effect on the flowability and printing quality of cementitious materials. Initially, CNTs in the form of PEG are made in powdered form. In this study, CNTs at concentrations of 0.1%, 0.2%, and 0.3% by weight of cement were dispersed in water with and without surfactants. SDBS and superplasticizers are used as a surfactant individually for the dispersion of CNTs. While a superplasticizer plays a vital role in improving flowability, SDBS is a high content anionic surfactant with detergency, moistening, foaming, and dispersity properties that is usually added during sonication. CNTs were effectively dispersed using a liquid processor ultrasonic wave mixer. The van der Waal forces between the CNTs can be distributed throughout the solutions by using the sonication technique. The primary focus of this work was on the first case, in which CNTs were placed in water without any surfactants and sonicated for 40 min with 40% amplitude maintained to evenly spread CNTs in water. Following sonication, the dispersed solution was added to dry ingredients such as cement and sand, and then mixed for 3 min to increase the paste's homogeneity. This process served as the foundation for adding CNTs to the basic mix of 3D printed cementitious material. Moving on to the subsequent case, SDBS was added to the CNTs solution, and the sonication procedure was repeated as previously stated. In the final case, a superplasticizer was used instead of SDBS, and a similar sonication and mixing procedure were followed. Fig. 2(a) and (b) show CNTs with superplasticizer in water before and after the sonication. These methodical approaches were taken to determine the best mix design for 3D printed cementitious materials by integrating CNTs into the basic mix.

2.3. Testing procedures

To examine the effect of CNTs in 3D printing of cementitious materials, various tests were conducted, such as printing quality, buildability, rheology, open time, compression, and three-point bending. The printing quality encompasses the assurance of structural integrity, surface finish, geometric accuracy, and consistency across the 3D printed layers (Kazemian et al., 2017). In printing quality test, one layer and two layers were printed based on the obtained mix designs. A ruler was used to measure the dimensions of layers, giving particular attention to the measurements of height and width at five different locations along their length. The average length, width, and height of three printed layers per mixture were determined and compared with CAD dimensions. In this

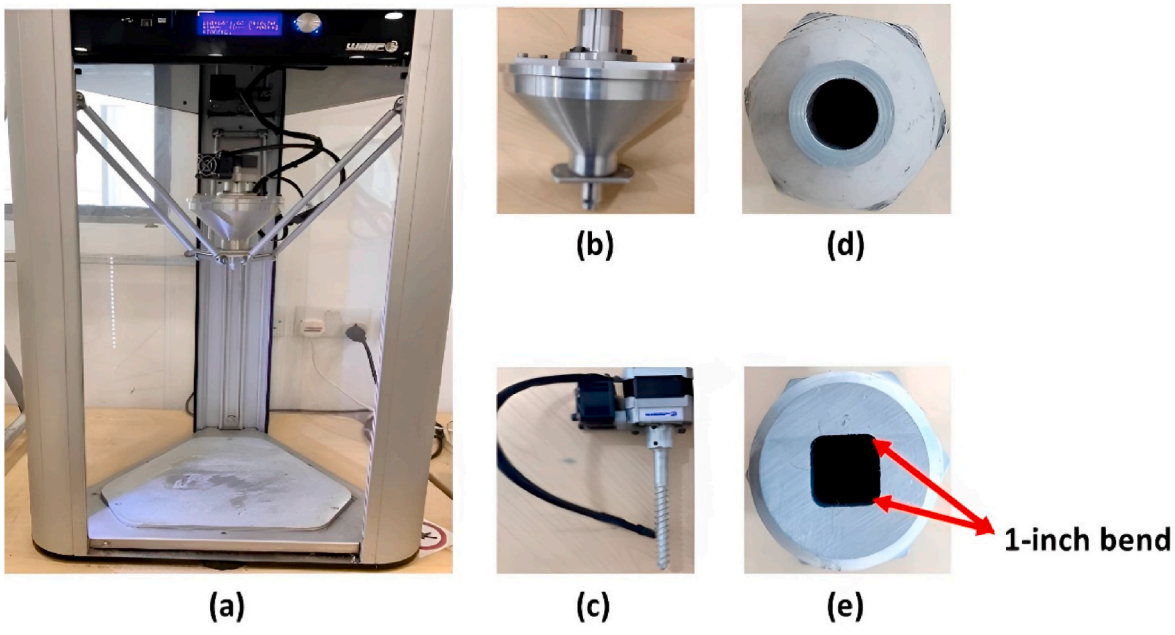

Fig. 1. (a) Delta WASP 3D printer system; (b) Extruder; (c) WASP motor; (d) 5 mm circular nozzle; and (e) 5 mm square nozzle with R-1 bend.

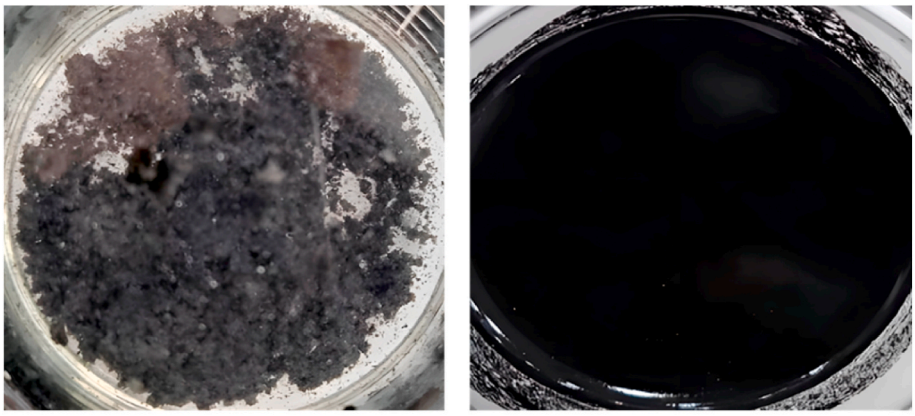

Fig. 2. CNTs with superplasticizer in water (a) before, and (b) after sonication.

study, the reference dimensions in the CAD design are 150 mm x 5 mm x 5 mm for the single layer and 150 mm x 5 mm x 10 mm for the double layer. The percentage error in dimensions of single and double layers were calculated using:

$$Percentage\ error\ (\%) = \left(\frac{Measured\ dimension\ -\ CAD\ dimension}{CAD\ dimension}\right) \times 100. \tag{1}$$

A buildability test was performed to evaluate constructability, i.e., the ability to print cementitious materials by continuously adding layers up to the required level without deforming or collapsing the newly printed components (Muthukrishnan et al., 2021; Ma et al., 2018). In this test, multiple layers were printed for each mixture up to its maximum height without collapsing or deforming using a CAD model with dimensions of 40 mm x 40 mm x 400 mm. A ruler was used to measure the maximum height attained by each sample. Three samples were performed for each mixture, and the average result was recorded. Simultaneously, an open-time test was performed to determine the time span during which the cementitious material remains extrudable, i.e., the period during which the material can be continuously extruded without blockage or collapse (Jo et al., 2020). In the open-time test, the duration was measured from the printing of the initial layer until the point where the printed specimen failed or collapsed upon reaching a specific height. It should be noted that this test was conducted simultaneously with the buildability test. Three trials were conducted for each mix, and the mean time in minutes was measured.

The rheological properties of various mixes were measured using an Anton Paar MCR-302 rheometer, as shown in Fig. 3(a). This device was used to measure the shear stress and viscosity at different shear rates. As depicted in Fig. 3(a), the bottom and top plates of the rheometer are profiled parallel plates with dimensions of 25 mm and 8 mm in diameter, respectively. The use of profiled parallel plates in the rheometer increases sensitivity, i.e., the ability to detect changes in the viscosity of the sample more precisely, and reduces sample slippage, resulting in better contact on the sample and preventing unwanted movement, thereby improving the accuracy of viscosity measurement. Initially, the cement mortar was prepared using the obtained mix proportion. A small portion of cement mortar was placed on the bottom plate connected to the rheometer. Later, the top plate was allowed to contact the specimen, maintaining a gap of 2 mm between both plates. Moreover, the temperature maintained for this test was 24 °C. The viscosity and shear stress at various shear rates were recorded until the sample failed contact with the top plate, i.e., when the sample got hardened. Three samples were considered for each printable mix, and average viscosity and shear stress were recorded.

Mechanical testing such as compression and three-point bending tests was conducted for 3D printed specimens using INSTRON and MTS universal testing machines to observe enhanced development in strength by adding CNTs to the printable mixes. Compressive strength tests were carried out for 3D printed cubes of size 50 mm x 50 mm x 50 mm according to the specification ASTM C109 (American Society for Testing and Materials. Committee C-1 on Cement, 2013). Flexural strength tests were performed using a three-point bending test for 3D printed beams of size 150 mm x 40 mm x 40 mm as per ASTM C348 (348M – 18, 2018). Fig. 3(b) and (c) illustrate the schematic diagram of the compression and three-point bending tests, along with the dimensions and loading direction with respect to the printing direction. It was important to highlight that the loading direction in the printed material was perpendicular to the 3D printed layer alignment. For both tests, 3D printed samples were first kept on a printed platform for 24 h. Subsequently, the samples were stored in a bag for 1, 7, and 28 days of dry curing. Three printed samples were tested for each case, and average compressive and flexural strengths were evaluated for the above mentioned days using

$$Compressive\ strength = \frac{P}{bd}, \tag{2}$$

$$Flexural\ strength = \frac{3FL}{2bd^2} \tag{3}$$

where P is the compressive force, F is the maximum applied force in three-point bending test, b and d are width and depth of the specimen's dimensions.

In order to perform microstructural analysis, samples of cement mortar with SF and CNTs were prepared. A layer of gold coating was applied to the surface of cement mortar using magnetron sputtering for 30 s in order to prevent charge accumulation during interactions with an electron beam. The coated cement mortar was then placed inside the Joel Field Emission Scanning Electron Microscope (FESEM). The examination entailed the observation of both the surface and cross-sectional views of the CNT-cement matrix. The flakes of the CNT-cement matrix were observed by adjusting the focus of the image in order to examine the dispersion and distribution of CNTs within the cement matrix. This method aids in assessing the effectiveness of CNTs in improving the mechanical properties and structural performance of cementitious materials.

3. Optimal mix designs and nozzle shapes

This section provides optimal printable mix designs for each category outlined in Table 1. Moreover, a comparison of two different nozzles based on printing quality was evaluated to determine the better nozzle shape for the Delta WASP 3D printer. To investigate the effect of adding

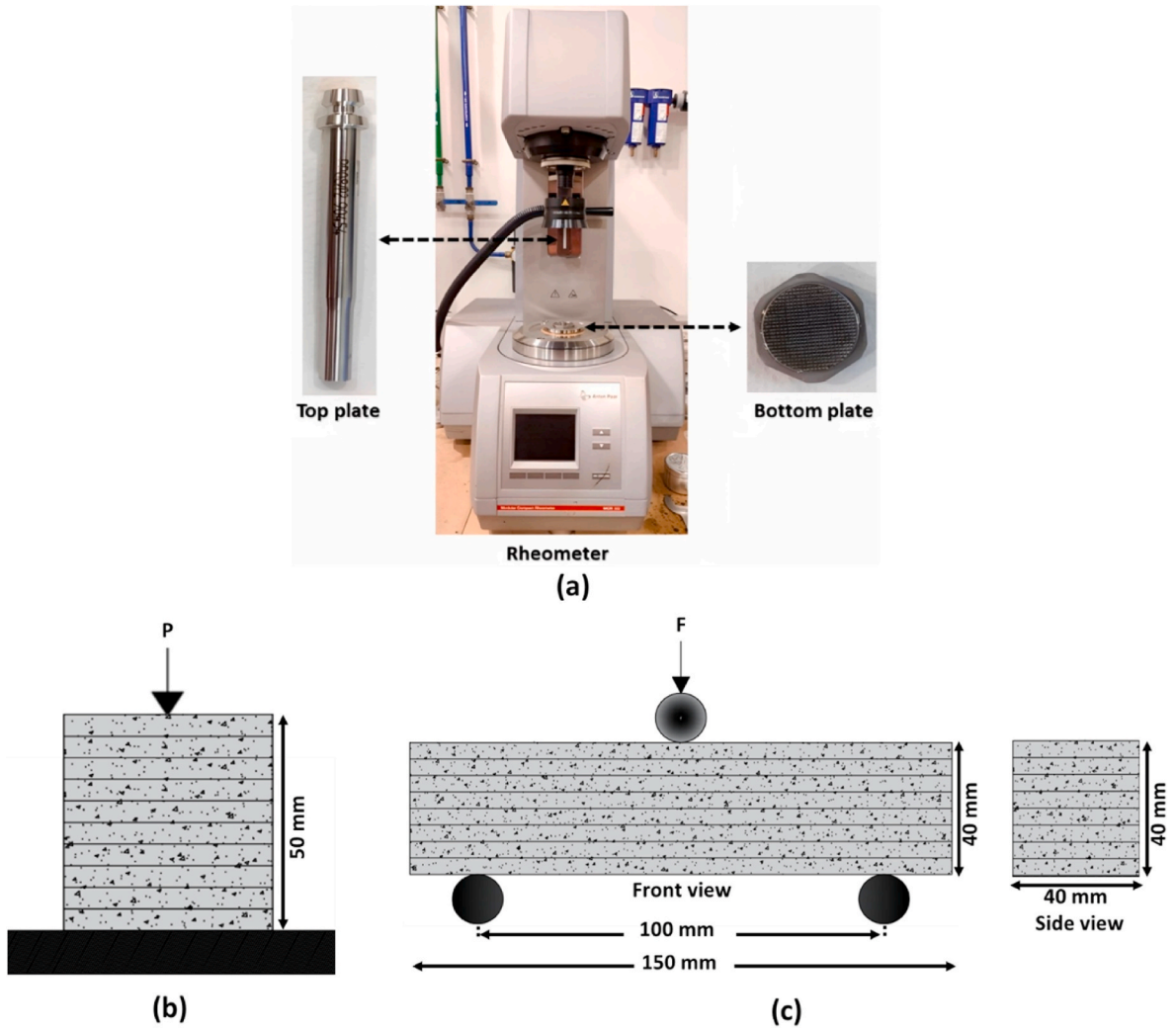

Fig. 3. Experimental tests: (a) Anti-Paar MCR rheometer with top and bottom profiled parallel plates; and Schematic diagram of loading directions for (a) compression test of cube, and (c) three-point bending test of beam.

CNTs to cementitious materials for 3D printing, the six categories of mixes were considered in this study, as summarized in Table 1. The optimal mix designs for these categories that are printable for the designed 3D printer were examined. Category-1 includes basic mixtures composed of cement, sand, and water. In Category-2 silica fume (SF) was added to the basic mix, whereas Category 3 incorporates CNTs without any surfactant. Moreover, Category-4 explores the influence of CNTs mixed with surfactant SDBS, whereas Category-5 integrates CNTs with a superplasticizer. Category-6 contains all of the components from Categories 2, 3, and 5, mainly SF, CNTs, and a superplasticizer. It should be emphasized that the CNTs were sonicated, with or without a surfactant, before being added to the dry ingredients based on their respective categories. This categorization enables a systematic investigation of various additive combinations in order to comprehend their impact on the properties of printed cementitious materials.

3.1. Optimal printable mix design for Category-1

The optimal printable mix design for Category-1, i.e., the basic mix consisting of cement, water, and sand, was determined by varying mix proportions with a water to cement (w/c) ratio ranging from 0.35 to 0.45, as shown in Table 2. The mix proportions were found through an iterative method due to the absence of specific guidelines for the mix design of cement-based materials in 3D printing. Furthermore, the selections were made while ensuring that the mix proportions would not cause blockages in the extruder while printing. Generally, blockages in 3D printing occur when cement mortar clogs the extruder due to inadequate flowability. Moreover, to improve flowability and stability throughout the printing process, 3D printing mixes with a high cement concentration were used. However, it might lead to higher shrinkage and cracking during curing. The decision to employ a high cement concentration (i.e., 50-60 %) was based on several considerations, including the desired qualities of the printed product, the printing technique using a small-scale nozzle, and the use of additives such as CNTs and SF to mitigate shrinkage and cracking (Yazdanbakhsh et al., 2012). Mix-3A was found to be the only printable mix proportion for Category-1 without blockage of the extruder during the extrusion process for both circular and square nozzles. Furthermore, using Mix-3A, by

Table 1
Categories of mixes considered in this study.

Category	Materials used for obtaining the mix proportions
Category-1	Cement, sand, and water
Category-2	Cement, sand, water, and SF
Category-3	Cement, sand, water, and CNTs
Category-4	Cement, sand, water, and CNTs with SDBS
Category-5	Cement, sand, water, and CNTs with superplasticizer
Category-6	Cement, sand, water, SF, and CNTs with superplasticizer

Table 2
Printability of the basic mix, i.e., Category-1, for square and circular nozzles.

Mix-ID	Cement (%)	Sand (%)	Water (%)	w/c	Printability condition
Mix-1A	60	19.00	21.00	0.35	Blockage
Mix-2A	60	17.20	22.80	0.38	Blockage
Mix-3A	60	16.60	23.40	0.39	Printable
Mix-4A	55	23.00	22.00	0.40	Blockage
Mix-5A	58	17.64	24.36	0.42	Blockage
Mix-6A	55	21.35	23.65	0.43	Too dilute
Mix-7A	50	30.00	20.00	0.45	Blockage

varying printing speeds from 15 mm/s to 30 mm/s, 25 mm/s was found to be suitable for the designed 3D printer as there was no blockage observed in printing and the printed layers were uniform and consistent. As a result, unless otherwise specified, Mix-3A was used as the control mix and 25 mm/s as the printing speed for the rest of the paper.

The printing quality for both circular and square nozzles was investigated for Mix-3A. Three samples of single and double layers were printed from both nozzles and compared with the dimensions in the CAD design. In general, the percentage errors for the length and width of both single and double layers were below 2% for both nozzles. Similarly, the percentage error for the height of the single layer was also found to be less than 2% as shown in Table 3. These findings indicate that the length and width of both layers, as well as the height of the single layer, closely match the dimensions specified in the CAD design. On the contrary, the errors in height for the double layer are more than 30.0% due to the deformation caused by pouring the second layer over the first layer. In particular, the percentage errors in the height of the double layer were lower for the circular nozzle, i.e., 38.0%, when compared with the square nozzle, i.e., 41.4%, respectively. This outcome indicates that the printing quality was enhanced by using the circular nozzle. Examples of the single and double layers printed using both nozzles are displayed in Fig. 4(a)-(d) for qualitative comparison. Fig. 4(a) and (b) show the top view of one-layer printed with circular and square nozzles, respectively, while Fig. 4(c) and (d) depict the front view of two-layers printed with each nozzle shape. After analysing one-layer and two-layers, more complex shapes, i.e., square and circular objects, were printed as illustrated in Fig. 4(e)-(h) using both nozzles. It was found that the printed shapes from the circular nozzle have a consistent and smooth surface compared to those from the square nozzle. In particular, the edges of the layers printed by the circular nozzle were consistent, whereas those generated by the square nozzle exhibited discernible irregularities i.e., layer edges were not uniform. Therefore, better printing quality was highlighted with the use of the circular nozzle than the square nozzle.

Multiple layers were printed using Mix-3A for both nozzle shapes, as shown in Fig. 5(a) and (b). Three samples were printed, and the average height was measured. It was found that an average height of 58 ± 4 mm was printed using the circular nozzle, in contrast to a 50 ± 5 mm height by the square nozzle. Moreover, the multiple-layer demonstration for both nozzles was carried out to observe the behaviour of the printed layers in the absence of any additives. It should be noted that the absence of additives in mix-3A caused the initial layers to become incapable of supporting the weight of subsequent layers. As a result, additives, including SF and CNTs, were added to the basic mixture to mitigate this issue.

Table 3
Summary of circular and square nozzles in terms of layer dimensions.

Dimensions	Reference dimension for one layer (mm)	One layer (mm)	Reference dimension for two layers (mm)	Two layers (mm)	Error in one layer (%)	Error in two layers (%)
5 mm circular nozzle						
Length	150.0	151.0	150.0	151.0	0.67	0.67
Width	5.0	5.036	5.0	5.061	0.72	1.22
Height	5.0	4.910	10.0	6.200	1.80	38.00
5 mm square nozzle						
Length	150.0	151.0	150.0	151.0	0.67	0.67
Width	5.0	5.080	5.0	5.062	1.6	1.24
Height	5.0	4.900	10.0	5.860	2.0	41.40

3.2. Optimal printable mix designs by adding CNTs

This section presents the optimal mix designs with the addition of CNTs and SF to the basic mix that are printable on the designed extruder and the 5 mm circular shape nozzle. The printable mix proportions were obtained for three types of mixes, i.e., the addition of only SF, only CNTs, and both SF and CNTs into the basic mix. Firstly, various mix proportions of Category-2 (i.e., cement, sand, water, and SF) as mentioned in Table 1 were tested to find the printable mix design, as summarized in Table 4. Mix-2B was found to be the only printable mix with a w/c ratio of 0.4. It was found that adding 5% SF to the basic mix lowers liquidity, enhances printability, and creates cohesion and stability for the initial printed layers. It was worth noting that, with the use of SF, the cement and water contents were slightly reduced compared to the basic mix of Mix-3A in Table 2.

Mix proportions were obtained by adding CNTs to the basic mix. It was found that adding CNTs without any surfactants, i.e., Category-3 in Table 2, resulted in blockage of the extruder due to improper CNTs dispersion and poor flowability. As a result, SDBS was added with CNTs to improve dispersion. Interestingly, there was further blockage in the extruder with the addition of SDBS, i.e., Category-4 in Table 2, due to poor flowability. The superplasticizer was thus added to improve the flowability of the mix. Table 5 presents various trials of mix proportions by varying concentrations of CNTs along with the superplasticizer, i.e., Category-5 in Table 2. The results indicated that the addition of the superplasticizer in concentrations of 0.4% and 0.7% to a CNTs solution of 0.1% and 0.2% significantly improves printing quality. Consequently, Mix-1C and Mix-3C were identified as the optimal printable designs for 3D printing with the addition of CNTs.

Moreover, the optimal printable mix design was examined for the mix proportion including both SF and CNTs in the basic mix, i.e., Category-6 in Table 2. Table 6 shows various mix proportion trials by varying the concentrations of SF, CNTs, and the superplasticizer. Mix-2D was found to be printable, having 5% of SF, 0.1% of CNTs, 0.5% of the superplasticizer, and a w/c ratio of 0.4. Hence, a total of five mixes were obtained from the categories listed in Table 2, namely Mix-3A, Mix-2B, Mix-1C, Mix-3C, and Mix-2D. These mixtures showed good flowability and prevented obstruction of materials inside the extruder and nozzle.

4. Results and discussion

This section includes the outcomes and discussion of fresh state properties, mainly printing quality, buildability, open time, and rheology of the obtained printable mix designs. Furthermore, the results of hardened state properties (mechanical properties) in terms of compressive strength, Young's modulus, and flexural strength were highlighted. Finally, the section presents the findings of the microstructural analysis of the CNT-cement matrix.

4.1. Effect of CNTs on printing quality

The influence of CNTs on printing quality is investigated by comparing all the printable mix designs with CNTs, i.e., Mix-1C (with 0.1% CNTs), Mix-3C (with 0.2% CNTs), and Mix-2D (with 5% SF and 0.1% CNTs), and those without CNTs, i.e., Mix-3A (without SF and

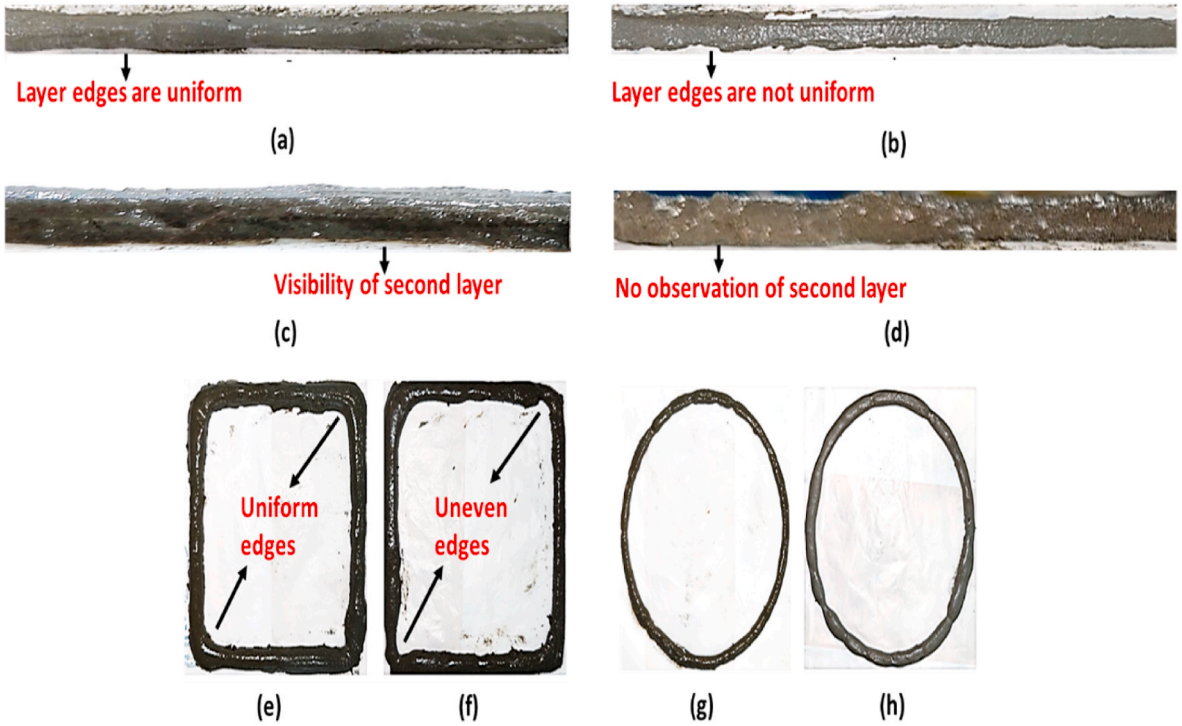

Fig. 4. Comparison appearance for Mix-3A: Top row shows the top view of the one-layer printing using (a) circular nozzle (b) square nozzle; middle row shows the front view of the two-layers using (c) circular nozzle (d) square nozzle; last row shows the square object using (e) circular nozzle (f) square nozzle; and circular object using (g) circular nozzle and (h) square nozzle.

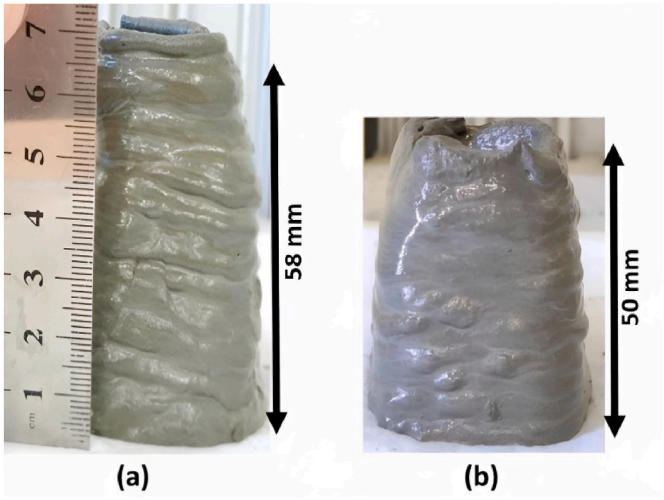

Fig. 5. Multiple layers printed using (a) circular nozzle, and (b) square nozzle of Mix-3A.

CNTs) and Mix-2B (with 5% SF). For all the printable mix designs, three samples for both single and double layers were printed. Examples of both layers for each printable mix design are displayed in Fig. 6. The average dimensions (i.e., length, width, and height) of three samples for each mix design are summarized in Table 7 along with the percentage errors computed by Eq. (1).

Overall, the percentage errors in the length and width for both layers were less than 1.3% for all the mixes. This indicates that the length and width of the printed layers are close to the dimensions in the CAD design, verifying the high accuracy of the proposed printable mix designs. Additionally, this finding was consistent with the research conducted by Kazemian et al. (2017), which concluded that the printing

Table 4
Printable mix design for the addition of SF into the basic mix.

Mix-ID	Cement (%)	Sand (%)	Water (%)	SF (%)	w/c	Printability condition
Mix-1B	55.0	18.55	21.45	5.0	0.39	Blockage
Mix-2B	55.0	18.00	22.00	5.0	0.40	Printable
Mix-3B	50.0	20.50	19.50	10.0	0.39	Blockage
Mix-4B	50.0	19.50	20.50	10.0	0.41	Blockage
Mix-5B	45.0	22.45	17.55	15.0	0.39	Blockage

quality assessment was satisfactory if the margins of error in the width of a single-layer print remained below 10% within a permissible range. There was no significant difference in the percentage errors for all printable mixes in length and width of both single and double layers, as shown in Fig. 7. However, variations were found in the height of both layers. The percentage errors in length and width for one and two layers are slightly decreased with the addition of SF and CNTs. Compared to Mix-3A, the percentage error in length and width of both layers of Mix-2B was very minor. However, the error in the single layer was reduced to 0.53% in length and 0.60% in width, and in the double layer, it was 0.53% in length and 0.60% in width due to the addition of CNTs. Interestingly, there was no significant difference in percentage error in the length and width of both layers with a variation of CNT content of 0.1% and 0.2%, respectively. In other words, Mix-1C, Mix-3C, and Mix-2D exhibited similar percentage errors in the length and width of both layers. On the other hand, the errors in height for the double layer were more than 30% because the second layer causes deformation when it is poured over the first layer. The percentage error dropped from 1.8% to 1% when SF and CNTs were added to the basic mixture in the context of one layer. Nevertheless, the primary focus was on the percentage

Table 5
Printable mix by varying percentages of CNTs and superplasticizer.

Mix-ID	Cement (%)	Sand (%)	Water (%)	CNTs *(% by cement weight)*	Super-Plasticizer (%)	w/c	Printability condition
Mix-1C	59.60	16.75	23.25	0.10	0.4	0.39	Printable
Mix-2C	59.00	17.00	23.00	0.10	1.0	0.39	Too dilute
Mix-3C	59.30	16.87	23.13	0.20	0.7	0.39	Printable
Mix-4C	59.00	17.00	23.00	0.20	1.0	0.39	Too dilute
Mix-5C	59.50	16.80	23.20	0.30	0.5	0.39	Blockage
Mix-6C	59.00	17.00	23.00	0.30	1.0	0.39	Blockage

Table 6
Printable mix by varying percentages of SF, CNTs and superplasticizer.

Mix-ID	Cement (%)	Sand (%)	Water (%)	SF (%)	CNTs *(% by cement weight)*	Super-Plasticizer (%)	w/c	Printability condition
Mix-1D	54.20	18.32	21.68	5.00	0.10	0.8	0.39	Blockage
Mix-2D	54.50	18.20	21.80	5.00	0.10	0.5	0.40	Printable
Mix-3D	50.00	20.00	20.00	9.50	0.10	0.5	0.39	Blockage
Mix-4D	54.20	18.32	21.68	5.00	0.20	0.8	0.39	Blockage
Mix-5D	54.50	18.20	21.80	5.00	0.20	0.5	0.40	Blockage
Mix-6D	50.00	20.00	20.00	9.50	0.20	0.5	0.39	Blockage

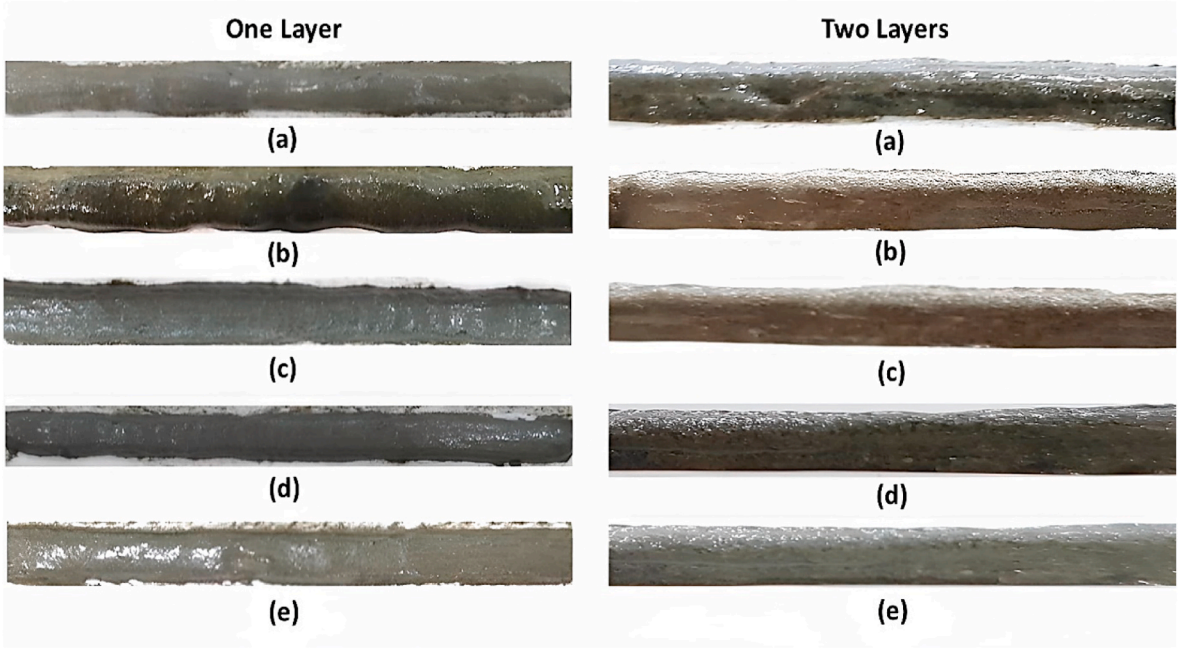

Fig. 6. Examples of the 3D printed layers for printing quality tests: Top view of one layer and front view of two layers for (a) Mix-3A, (b) Mix-2B, (c) Mix-1C, (d) Mix-3C, and (e) Mix-2D.

error in the heights of two layers. After adding SF to the control mixture of Mix-3A, the double layer's height inaccuracy dropped from 38% in Mix-3A (without SF) to 35% in Mix-2B (with SF). Most importantly, the addition of CNTs reduced significant deformation in the 3D printed layers, consequently reducing percentage errors in height. Specifically, for Mix-1C and Mix-3C, the height of the double layer decreased to 33% and 31%, respectively, in comparison to the baseline of 38% in Mix-3A. A more substantial reduction in the error percentage was noticeable in the combination of SF and CNTs, Mix-2D, reaching 30% for the height of two layers, thereby contributing to an improvement in printing quality. The reduction of the error in height of both layers was ascribed to the addition of CNTs into the cement mortar, which supported the weight exerted on each successive layer during the pouring process, thus ensuring layer uniformity.

In addition, square shapes with a side length of 50 mm and circular shapes with a diameter of 50 mm were printed for all possible mixtures, as shown in Fig. 8(a)-(e). Notably, the dimensions of the square and circular shapes were similar to those in the CAD model. These printed objects enabled a more detailed display of the printed shapes, beyond the single and double layers. The transition to closed-loop printing, shown by the single layer of square and circular shapes, provides a more comprehensive evaluation of printing quality across various mixes. However, it is worth noting that, by visualization, the printed shapes were uniform for all mixes.

In order to perform compression tests, 50 mm cubes for all printable mix designs were printed, as displayed in Fig. 9. For the control mix of Mix-3A, as shown in Fig. 9(a), the dimensions of the bottom, top, and height of the printed sample are respectively 65 mm, 53 mm, and 46 mm, which significantly deviated from 50 mm of the CAD dimension. Moreover, the printed sample shows bulging from the bottom side, which causes an increase in the dimension of the lower side. On the other hand, Mix-2B, Mix-1C, Mix-3C, and Mix-2D did not result in bulging from their bottom sides, as depicted in Fig. 9 (b)-(e). In contrast to Mix-3A, the addition of SF and CNTs prevents the protrusion of the

Table 7
Printing quality of single and double layers for the printable mix designs.

Mix-ID	Length (mm)	Width (mm)	Height (mm)	Error in length (%)	Error in width (%)	Error in height (%)
Reference dimension for one layer – 150 mm x 5 mm x 5 mm						
Mix-3A	151.0	5.036	4.910	0.67	0.72	1.80
Mix-2B	150.9	5.035	4.920	0.60	0.70	1.60
Mix-1C	150.8	5.030	4.920	0.53	0.60	1.60
Mix-3C	150.8	5.030	4.940	0.53	0.60	1.20
Mix-2D	150.8	5.030	4.950	0.53	0.60	1.00
Reference dimension for two layers – 150 mm x 5 mm x 10 mm						
Mix-3A	151.0	5.061	6.200	0.67	1.22	38.0
Mix-2B	150.9	5.060	6.500	0.60	1.20	35.0
Mix-1C	150.8	5.050	6.700	0.53	1.00	33.0
Mix-3C	150.8	5.050	6.900	0.53	1.00	31.0
Mix-2D	150.8	5.040	7.000	0.53	0.80	30.0

cubes from their bottom side. The dimensions (top, bottom, and height) measured for the printed cubes in Mix-2B, Mix-1C, Mix-3C, and Mix-2D manifest an error of less than 2%. Notably, the dimensions of these printed cubes were almost indistinguishable from the dimensions in the CAD design and were therefore utilized for the compressive strength testing in Section 4.4.

4.2. Effect of CNTs on buildability and open time

The buildability tests were carried out for the obtained printable mixes, i.e., Mix-3A, Mix-2B, Mix-1C, Mix-3C, and Mix-2D. Three samples per mix design were considered, and buildability values were obtained by measuring the average height at which samples exhibit failure or collapse. The CAD model utilized for this test has the following dimensions: 40 mm long, 40 mm wide, and 400 mm high. Fig. 10(a) illustrates the variation in height for different printable mixes. Overall, adding SF and CNTs significantly improved the buildability compared with the control mix of Mix-3A as shown in Fig. 10(b). The buildability of Mix-2B (5% SF) was enhanced by 18% compared with the control mix, indicating the SF enhanced stability of the initially printed layers. Moreover, further improvement was found by adding 0.1% CNTs (Mix-1C) and 0.2% CNTs (Mix-3C) by 57% and 81%, respectively. This indicates that CNTs contribute to the stability and cohesion of the printed layers by sonicating them in order to achieve proper dispersion and flowability. In addition, Mix-1C and Mix-3C resulted in enhancements of buildability by 34% and 55%, respectively, when compared to Mix-2B. Furthermore, varying CNT concentrations from 0.1% to 0.2%, enhanced the buildability by 15%. The addition of 5% SF and 0.1% CNTs together (Mix-2D) resulted in an improvement in buildability of 74% when compared with the control mix and 49% when compared with Mix-2B. Interestingly, Mix-2D resulted in a smaller reduction in buildability than Mix-3C and a slight increase compared with Mix-1C. The number of layers printed with Mix-3A ranged from 7 to 10 layers, but increased to 12-15 layers when 5% SF (Mix-2B) was added to the basic mixture. On the other hand, adding CNTs to the control mix resulted in an increase in printed layers. As an illustration, Mix-1C (0.1% CNTs) resulted in 17-20 layers, whereas Mix-3C (0.2% CNTs) achieved the highest number of printed layers, i.e., 20-25 layers. Notably, Mix-2D was slightly lesser than Mix-3C, attaining 20-23 layers.

An open time test was carried out simultaneously by predicting the duration taken by the sample to collapse. The duration of printing increases with an increase in buildability for all printable mixes, as shown in Fig. 10(b). The buildability of Mix-3C was higher when compared to other mixes, i.e., reaching a maximum height of 105 mm within a duration of 22 min, resembling the longest open time without any blockage in the extruder or nozzle. This enhancement was attributed to the presence of CNTs in the cement mortar, which supports the weight imposed on each layer during the pouring of subsequent layers, resulting in uniform layers. Remarkably, CNTs, along with superplasticizer, enhance the flow properties and cohesion of cementitious material by facilitating better inter-particle interaction, resulting in smoother extrusion and improved layer adhesion during the printing process.

4.3. Rheology of the printable mixes

The rheology test was performed for all the printable mixes, i.e., Mix-3A, Mix-2B, Mix-2D, Mix-1C, and Mix-3C. Shear stress (kPa) and dynamic viscosity (kPa-sec) were measured at different shear rates. Three samples were examined for each printable mix, and their average was taken into consideration. Fig. 11(a) depicts a logarithmic curve of viscosity against shear rate. It was found that with an increase in shear rate,

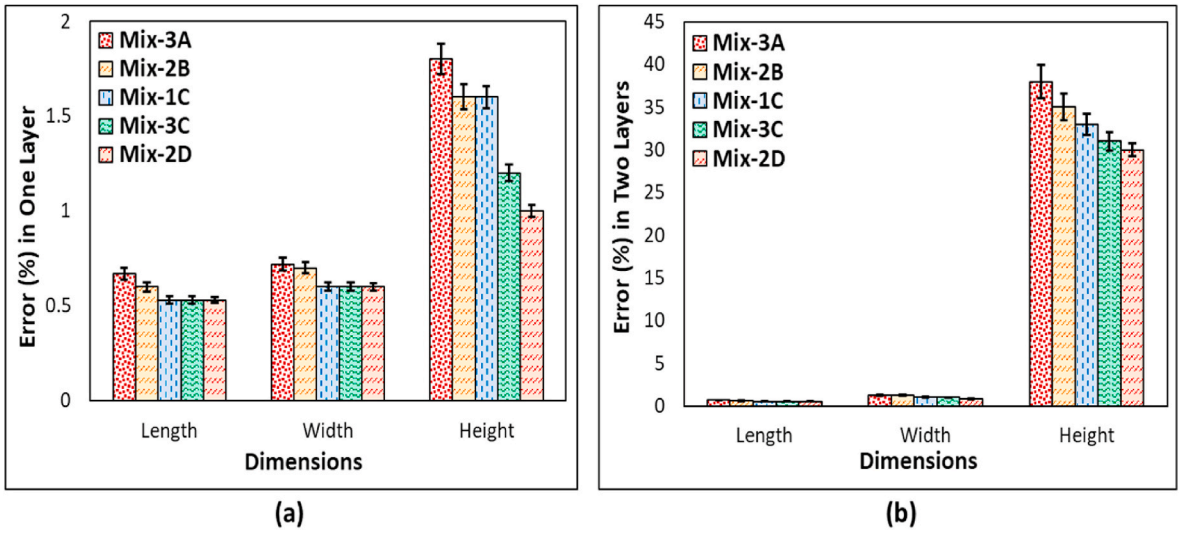

Fig. 7. Percentage error in dimensions (i.e., length, width, and height) of (a) one layer; and (b) two layers of Mix-3A, Mix-2B, Mix-1C, Mix-3C, and Mix-2D compared to the CAD model.

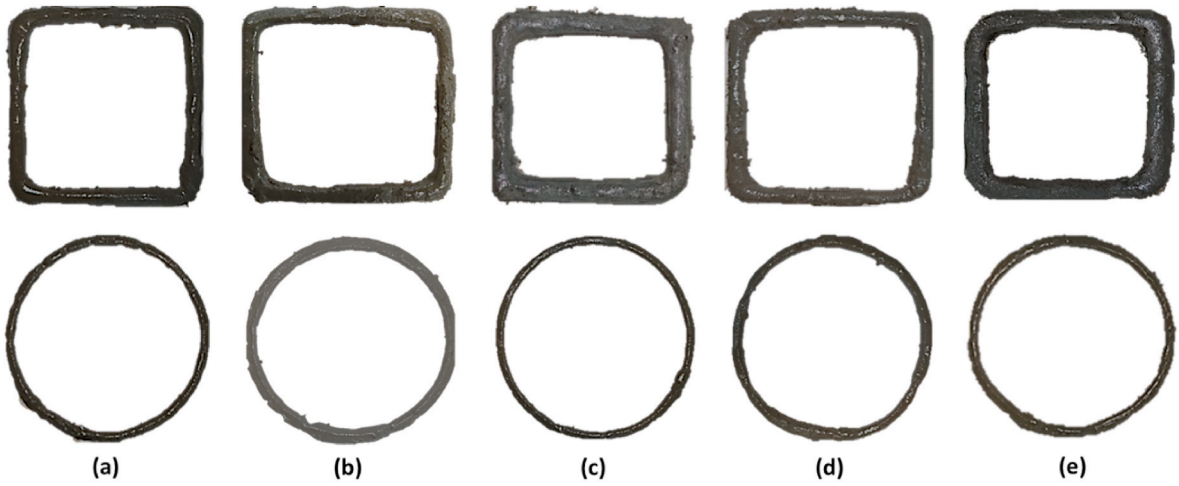

Fig. 8. Square and circular shapes of (a) Mix-3A (b) Mix-2B; (c) Mix-1C; (d) Mix-3C; and (e) Mix-2D.

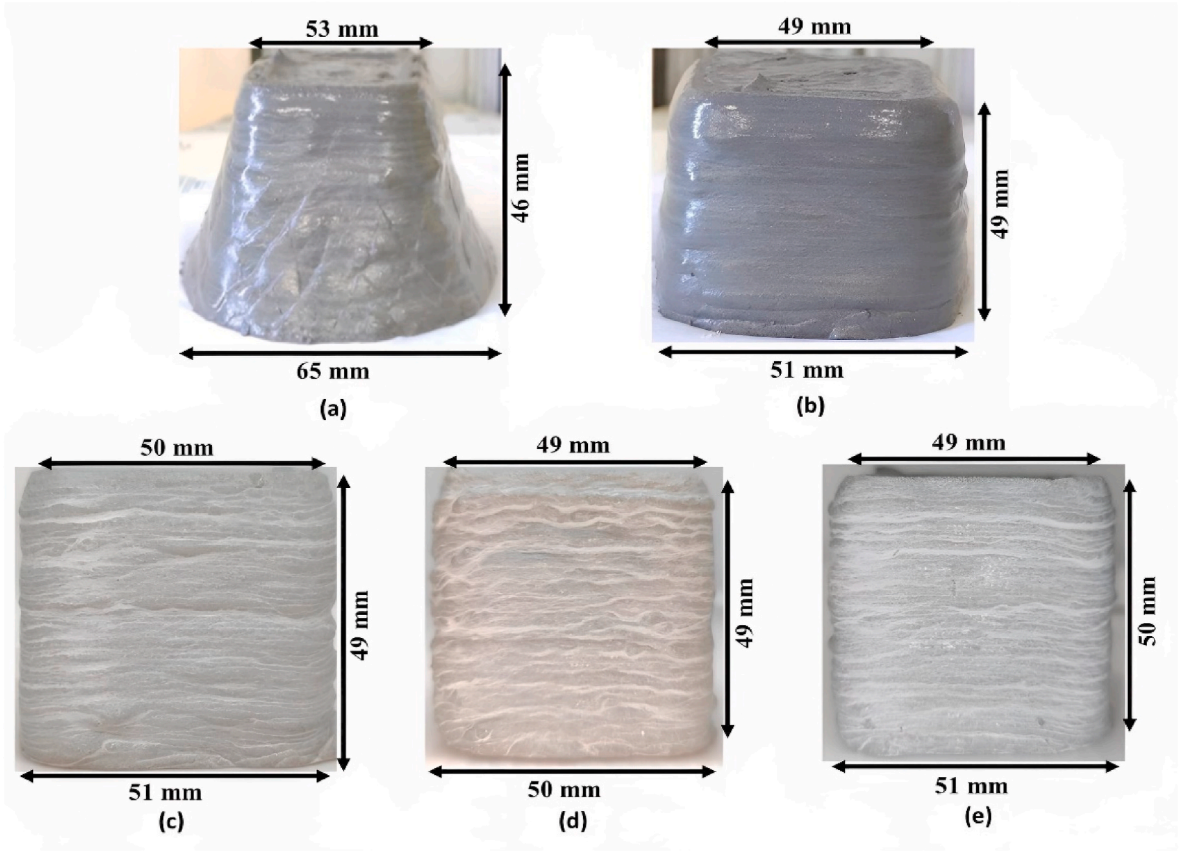

Fig. 9. Printed cubes for (a) Mix-3A; (b) Mix-2B; (c) Mix-1C; (d) Mix-3C; and (e) Mix-2D.

there was a noticeable reduction in viscosity, a behaviour commonly known as shear thinning. Fig. 11(b) shows the relationship between shear stress and shear rate, showing an initial increase in shear stress with the rise in shear rate and a subsequent reduction attributed to sample failure (i.e., the sample losing contact with the top plate). From Fig. 11(a) and (b), it becomes evident that Mix-3A consistently exhibits lower viscosity compared to Mix-2B across all shear rates. This suggests that the addition of SF contributes to an increase in viscosity. Moreover, the viscosity was reduced due to the inclusion of CNTs along with superplasticizer in the basic mix, as observed in Mix-1C, Mix-3C, and Mix-2D. Furthermore, at lower shear rates, Mix-2D exhibits lower viscosity compared to Mix-1C and Mix-3C. However, beyond a critical shearing rate, the viscosity of Mix-2D was found to increase, attributed to the intrusion of SF into the mix. It should be noted that the CNTs get aligned in the direction of the flow of material, reducing resistance and facilitating a uniform flow of cementitious materials through the printing nozzle, thereby improving the stability of the printed layers. Additionally, effective dispersion of CNTs in the cement mixture enhanced their interaction with the cement matrix, thereby preventing agglomeration and promoting uniform distribution. This uniform dispersion resulted in an improvement in the flow properties of the cementitious materials.

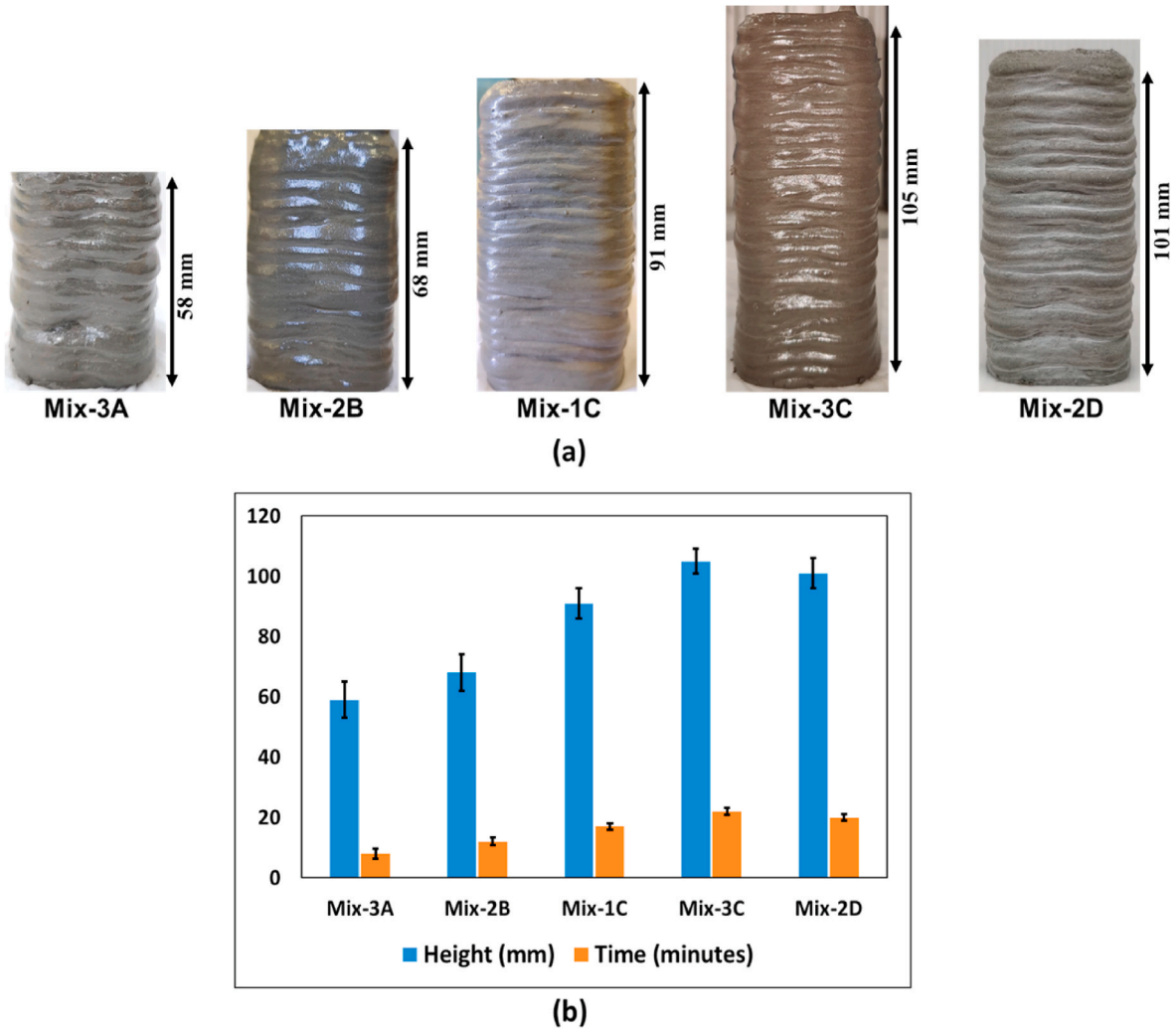

Fig. 10. (a) 3D printed samples used for buildability test; and (b) Height of 3D printed samples and open time for printable mixes.

4.4. *Effect of CNTs on the mechanical properties*

The influence of CNTs on compressive strength, Young's modulus, and flexural strength was investigated for the printable mix designs. Since Mix-3A was deemed unsuitable for mechanical testing due to the presence of protrusions from the lower side of the cube, Mix-2B (mixed with 5% SF) was considered the control mix to facilitate comparisons in mechanical properties with mixtures containing CNTs. A compressive strength test was conducted for 3D printed cubes using Mix-2B, Mix-1C, Mix-3C, and Mix-2D at 1, 7, and 28 days of curing, as illustrated in Fig. 12(a). The average compressive strength of three samples for each printable mix is shown in Fig. 12(b). Overall, the addition of CNTs increases compressive strength when compared with the control mix (Mix-2B). The comparison of Mix-1C and Mix-3C clearly showed an increase in compressive strength with increasing CNTs concentrations from 0.1% to 0.2%. Specifically, the compressive strength of Mix-3C (0.2% CNTs) was improved by 12%, 21%, and 25% at 1, 7, and 28 days, respectively, when compared with Mix-1C (0.1% CNTs). Moreover, adding 5% SF and 0.1% CNTs, i.e., Mix-2D, resulted in a smaller reduction in compressive strength than Mix-3C (0.2% CNTs) and a slight increment compared with Mix-1C (0.1% CNTs). When compared with Mix-2B, the compressive strength was increased by 51%, 68%, and 66% with respect to 1 day for Mix-1C, Mix-3C, and Mix-2D, whereas at 7 days it was 51%, 83%, and 72%, respectively. The compressive strength at 28 days was improved by 37%, 72%, and 55% for Mix-1C, Mix-3C, and Mix-2D, respectively. Fig. 12(c) depicts Young's modulus with respect to curing days (i.e., 1, 7, and 28). It was found that the Young's modulus also increases with increasing CNT content, from 0 to 0.2%. In comparison to Mix-1C, the Young's Modulus of Mix-3C was enhanced by 9%, 21%, and 20% at 1, 7, and 28 days, respectively. Interestingly, Mix-2D resulted in a slighter reduction in Young's modulus than Mix-3C and a smaller improvement over Mix-1C. When compared to Mix-2B, Young's modulus was increased by 35%, 48%, and 39% in the early stage (i.e., 1 day) for Mix-1C, Mix-3C, and Mix-2D, respectively, whereas at 7 days it was 22%, 47%, and 30%. The Young's modulus at 28 days was enhanced by 20%, 43%, and 27% for Mix-1C, Mix-3C, and Mix-2D, respectively. Relatively higher compressive strength and Young's modulus were obtained for Mix-3C due to the higher content of CNTs, i.e., 0.2% CNTs, that try to bond with the cement matrix, causing an enhancement in strength.

To study the effect of CNTs on flexural strength, three-point bending tests were performed using 3D printed beams with a size of 150 mm x 40 mm x 40 mm, as illustrated in Fig. 13(a). Three samples for each mix design were printed and cured for 1, 7, and 28 days. The mean flexural strength of three samples was computed using Eq. (3). Fig. 13(b) shows the increase in flexural strength with the increase in concentrations of CNTs for all three curing days. When compared to Mix-2B (acting as a control mix), the flexural strength was improved by 70%, 118%, and 85% at 1 day for Mix-1C, Mix-3C, and Mix-2D, respectively, and by 44%, 80%, and 63% at 7 days. The flexural strength at 28 days was increased by 68%, 99%, and 76% for Mix-1C, Mix-3C, and Mix-2D, respectively, as compared to Mix-2B. In comparison to Mix-1C, the flexural strength of

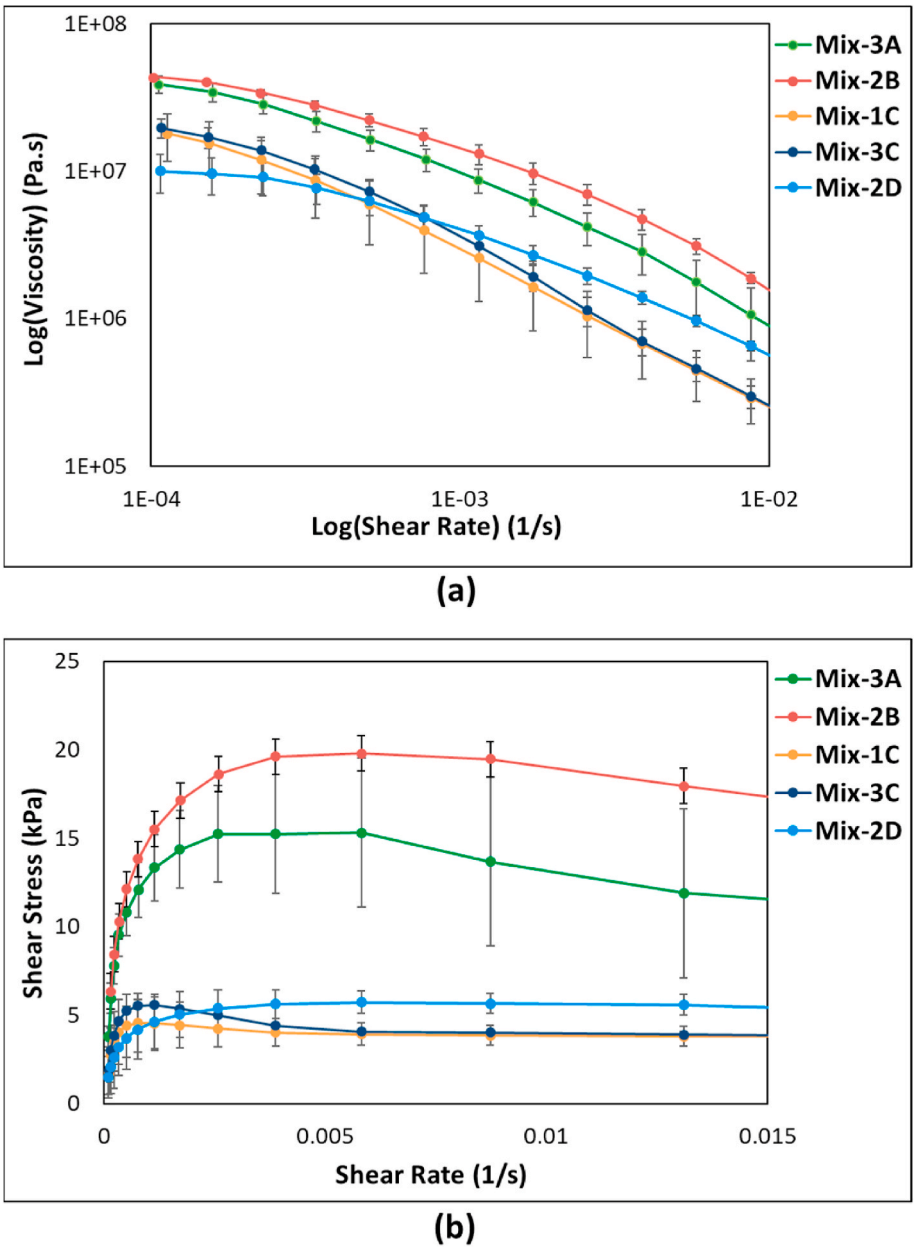

Fig. 11. (a) Viscosity vs. shear rate (logarithmic plot); and (b) Shear stress vs. shear rate.

Mix-3C was enhanced by 29%, 25%, and 19% at 1, 7, and 28 days, respectively. Hence, the flexural strength of Mix-3C was found to be higher than that of other mixes as it contains a higher content of CNTs. Interestingly, adding 5% SF and 0.1% CNTs in Mix-2D resulted in higher strength than 0.1% CNTs in Mix-1C and lower strength than 0.2% CNTs in Mix-3C.

The improved mechanical properties observed in 3D printed cement mortar with 0.2% CNTs were attributable to a number of important factors. Firstly, CNTs serve as effective reinforcing agents in the cementitious matrix. Moreover, the sonication process resulted in a uniform dispersion of CNTs throughout the matrix, preventing the agglomeration of material and enhancing their reinforcing properties. In addition, microstructural flaws such as voids and fractures were mitigated through nanoscale bridging of CNTs in the cement matrix as shown in Fig. 14, thereby limiting the propagation of cracks. Lastly, the improved printing quality achieved by assessing proper mix proportions resulted in a better interfacial bond between CNTs and cement matrix, resulting in uniform load transfer and thereby strengthening 3D-printed cement mortars.

4.5. *Microstructural analysis*

The effect of CNTs on the cementitious materials was examined by analyzing their microstructural characteristics using scanning electron microscope (SEM) images. Fig. 14(a) shows the microstructure of SF embedded in cement paste. The ultrafine particle size of SF facilitates effective interaction with the cement matrix and contributes to an improvement in printing quality by enhancing the cohesion and stability of the initially printed layers. It was important to emphasize that observing CNTs on the surface without fracture proved to be challenging. As a result, fracture surfaces were investigated to better understand the crack bridging impact of CNTs within the cement matrix. Fig. 14(b) shows nanoscale crack bridging of CNTs in the cement matrix for Mix-1C (i.e., 0.1% CNTs), while Fig. 14(c) and (d) depict two distinct regions of CNTs bridging in the cementitious matrix for Mix-3C (i.e., 0.2% CNTs). This methodology facilitated a comprehensive analysis of the role of CNTs in enhancing the mechanical strength of the material at the nanoscale. Although their diameter ranges from 10 nm to 25 nm,

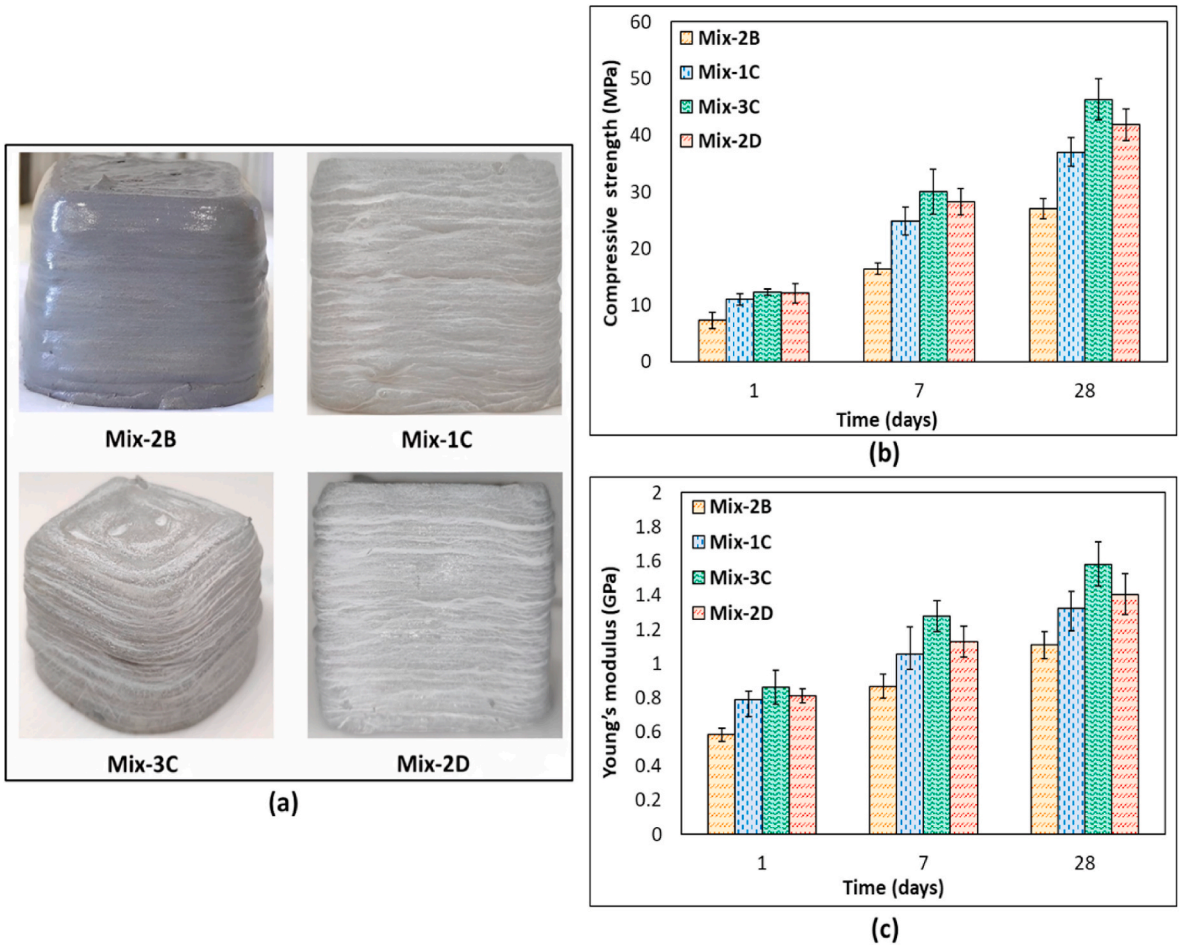

Fig. 12. (a) 3D printed cubes of side 50 mm for printable mix designs; (b) Compressive strength; and (c) Young's modulus of 3D printed cubes at 1, 7, and 28 days.

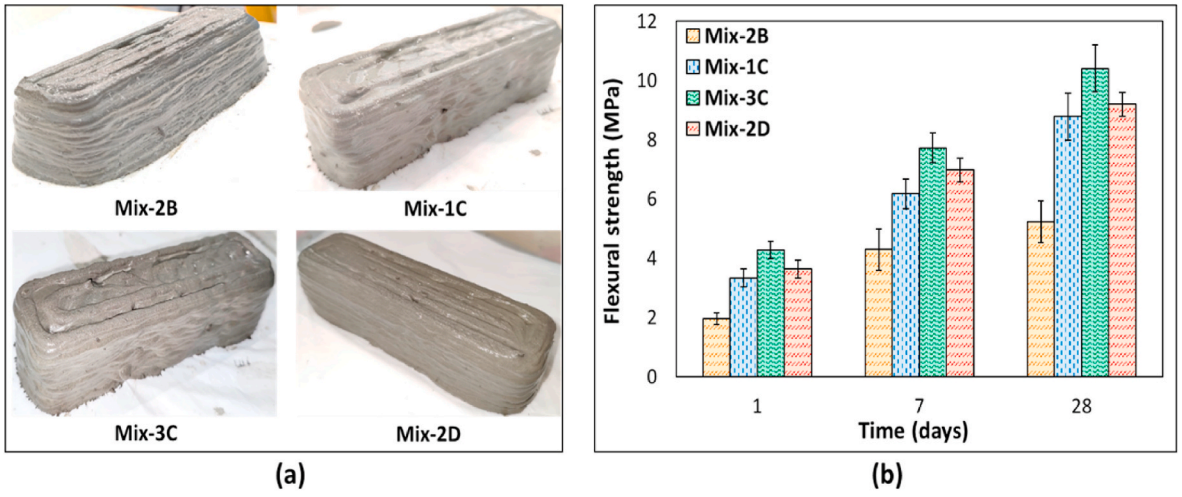

Fig. 13. (a) 3D printed beams with the size of 150 mm x 40 mm x 40 mm for printable mix designs; and (b) Flexural strength of 3D printed cubes at 1, 7, and 28 days.

CNTs demonstrate the ability to traverse wide fissures due to their high aspect ratio. The observed crack bridging effect of CNTs within the cement matrix, facilitated by ensuring their proper dispersion and flowability, considerably improves the mechanical properties of 3D printed structures. This enhancement extends beyond strength to entire mechanical performance, revealing the potential of CNTs as a key reinforcement in 3D printing of cementitious materials.

5. Conclusions

This study highlights the importance of CNTs in the 3D printing of cementitious materials. Optimal mix designs were obtained for the control mix as well as mixes incorporating SF, CNTs, and a combination of both CNTs and SF. Furthermore, two nozzle shapes, square and circular, were designed and fabricated, and their effect on printing quality and buildability was assessed using the control mix. The impact of CNTs

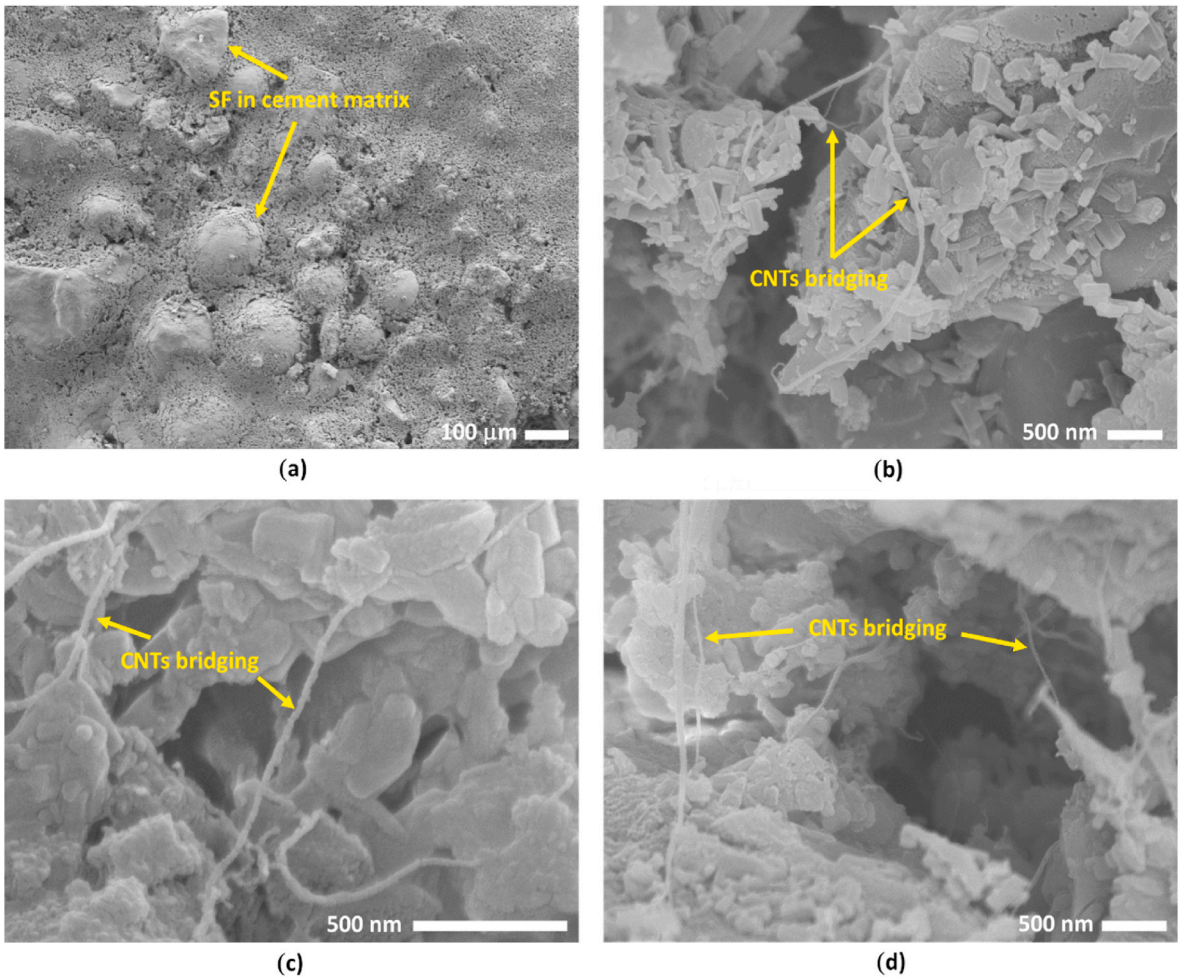

Fig. 14. SEM images showing (a) SF (Mix-2B) in the cement matrix; Nanoscale bridging of CNTs on the fracture surfaces in the cement matrix for (b) 0.1% CNTs (Mix-1C), and (c) 0.2% CNTs (Mix-3C), and d) Another view of 0.2% CNTs (Mix-3C).

on printing quality, buildability, open time, rheology, and mechanical properties was quantitatively evaluated and compared with the results of the control mix. The findings of this study are summarized as follows:

- The circular nozzle with a 5 mm diameter was found to be optimal for 3D printing as it provides a smooth, uniform surface and consistent extrusion for printed layers when compared to the square nozzle with 5 mm sides. Furthermore, the absence of additives in the mix resulted in the initial layers being incapable of providing sufficient support to the subsequent layers. As a result, additives were added to cementitious materials. Moreover, the optimal mix proportions were established by adding CNTs along with superplasticizer to the control mix with the aid of the sonication process to disperse CNTs more effectively at higher concentrations (specifically, 0.1% and 0.2% of the weight of cement).
- The addition of CNTs along with superplasticizer in cement mortar improved the printability, buildability, and rheology of the mix, particularly for 0.2% CNTs (by weight of cement). Compared to the control mix, the error in height of two-layers was reduced from 38% to 30%. Similarly, the buildability was improved by 81%, while the rheology properties exhibited shear thinning behaviour with lower viscosity, resulting in improved flowability of cementitious material.
- Increasing the concentration of CNTs from 0 to 0.2% resulted in a considerable enhancement in compressive and flexural strengths as well as Young's modulus. When compared to the mix containing SF, adding 0.2% CNTs by weight of cement increased the compressive strength by 68%, 83%, and 72% at 1, 7, and 28 days of curing, respectively. Concurrently, Young's modulus experienced growth by 48%, 47%, and 43%. Furthermore, the flexural strength exhibited remarkable enhancements of 118%, 80%, and 99% compared to the mix with SF. The improved mechanical properties were attributed to CNTs reinforcing the cementitious matrix, minimizing macro cracks and voids in printed layers, and limiting CNT agglomeration in the cement matrix through uniform dispersion using sonication.
- According to the microstructural investigation, nanoscale crack bridges were formed by CNTs at concentrations of 0.1% and 0.2% within the cement matrix. These bridges form a network-like structure (mostly fibres) that acts as reinforcement, increasing the cohesion and mechanical properties of the cementitious material.

In general, CNTs can affect the anisotropic behaviour of mechanical properties in 3D printed cement-based materials by means of alignment in the printed layers, reinforcement, dispersion, interfacial bonding, and printability. Understanding these impacts is critical for enhancing the performance of 3D printed concrete structures. To expand the scope of research, the impact of CNTs on the anisotropic behaviour of their mechanical properties should be investigated. Furthermore, research into the durability of these cementitious composites with various CNT dosages is required. Moreover, the effect of CNTs can be studied using a large scale 3D printer by upscaling the mix formulation. However, several challenges must be addressed, such as ensuring constant material characteristics and quality control over large production volumes, managing increased equipment and operational expenses, and resolving concerns related to material flow, viscosity, and curing rates. This

investigation allows researchers to optimize CNT integration in cementitious materials for improved mechanical performance and durability.

CRediT authorship contribution statement

Mohd Mukarram Ali: Formal analysis, Investigation, Methodology, Validation, Visualization, Writing – original draft, Writing – review & editing. **Ghaith Nassrullah:** Resources, Writing – review & editing. **Rashid K. Abu Al-Rub:** Funding acquisition, Supervision, Writing – review & editing. **Bashar Al-Khaswaneh:** Funding acquisition, Supervision, Writing – review & editing. **Seyed Hamidreza Ghaffar:** Resources, Writing – review & editing. **Tae-Yeon Kim:** Writing – review & editing, Writing – original draft, Validation, Supervision, Resources, Project administration, Methodology, Investigation, Funding acquisition, Conceptualization, Formal analysis.

Declaration of competing interest

The authors declare that they have no known competing financial interests or personal relationships that could have appeared to influence the work reported in this paper.

Data availability

Data will be made available on request.

Acknowledgements

The authors acknowledge research funding from Advanced Digital & Additive Manufacturing (ADAM) center in Khalifa University (No. 8474000163).

References

348M – 18, 2018. Standard Test Method for Flexural Strength of Hydraulic-Cement Mortars. ASTM C 348/C, West Conshohocken, PA (n.d.).

Abu Al-Rub, R.K., Ashour, A.I., Tyson, B.M., 2012a. On the aspect ratio effect of multi-walled carbon nanotube reinforcements on the mechanical properties of cementitious nanocomposites. Construct. Build. Mater. 35, 647–655. https://doi.org/10.1016/j.conbuildmat.2012.04.086.

Abu Al-Rub, R.K., Tyson, B.M., Yazdanbakhsh, A., Grasley, Z., 2012b. Mechanical properties of nanocomposite cement incorporating surface-treated and untreated carbon nanotubes and carbon nanofibers. J. of Nanomech. and Micromech 2 (1), 1–6. https://doi.org/10.1061/(ASCE)NM.2153-5477.0000041.

Abubakre, O.K., Medupin, R.O., Akintunde, I.B., Jimoh, O.T., Abdulkareem, A.S., Muriana, R.A., et al., 2023. Carbon nanotube-reinforced polymer nanocomposites for sustainable biomedical applications: a review. J. Sci.: Adv. Mater. and Devices, 100557. https://doi.org/10.1016/j.jsamd.2023.100557.

American Society for Testing and Materials. Committee C-1 on Cement, 2013. Standard test method for compressive strength of hydraulic cement mortars (using 2-in. Or [50-mm] Cube Specimens). ASTM Int.

Arash, B., Wang, Q., Varadan, V.K., 2014. Mechanical properties of carbon nanotube/polymer composites. Sci. Rep. 4 (1), 6479. https://doi.org/10.1038/srep06479.

Asprone, D., Auricchio, F., Menna, C., Mercuri, V., 2018. 3D printing of reinforced concrete elements: technology and design approach. Construct. Build. Mater. 165, 218–231. https://doi.org/10.1016/j.conbuildmat.2018.01.018.

ASTM C 1240/C 1240M – 18, 2020. Standard Specification for Silica Fume Used in Cementitious Mixtures, Elkem ASA, Vaagsbygd, Kristiansand, Norway (n.d.).

Baduge, S.K., Navaratnam, S., Abu-Zidan, Y., McCormack, T., Nguyen, K., Mendis, P., et al., 2021. Improving performance of additive manufactured (3D printed) concrete: a review on material mix design, processing, interlayer bonding, and reinforcing methods. Structures 29, 1597–1609. https://doi.org/10.1016/j.istruc.2020.12.061.

Balaji, K.V., Shirvanimoghaddam, K., Naebe, M., 2024. Multifunctional basalt fiber polymer composites enabled by carbon nanotubes and graphene. Composites, Part B 268, 111070. https://doi.org/10.1016/j.compositesb.2023.111070.

Bikas, H., Stavropoulos, P., Chryssolouris, G., 2016. Additive manufacturing methods and modelling approaches: a critical review. Int. J. Adv. Manuf. Technol. 83, 389–405. https://doi.org/10.1007/s00170-015-7576-2.

Buswell, R.A., Da Silva, W.L., Bos, F.P., Schipper, H.R., Lowke, D., Hack, N., et al., 2020. A process classification framework for defining and describing Digital Fabrication with Concrete. Cement Concr. Res. 134, 106068 https://doi.org/10.1016/j.cemconres.2020.106068.

Casagrande, L., Esposito, L., Menna, C., Asprone, D., Auricchio, F., 2022. Effect of testing procedures on buildability properties of 3D-printable concrete. Construct. Build. Mater. 245, 118286 https://doi.org/10.1016/j.conbuildmat.2020.118286.

Chougan, M., Ghaffar, S.H., Jahanzat, M., Albar, A., Mujaddedi, N., Swash, R., 2020. The influence of nano-additives in strengthening mechanical performance of 3D printed multi-binder geopolymer composites. Construct. Build. Mater. 250, 118928 https://doi.org/10.1016/j.conbuildmat.2020.118928.

Chougan, M., Ghaffar, S.H., Sikora, P., Chung, S.Y., Rucinska, T., Stephan, D., et al., 2021. Investigation of additive incorporation on rheological, microstructural and mechanical properties of 3D printable alkali-activated materials. Mater. Des. 202, 109574 https://doi.org/10.1016/j.matdes.2021.109574.

Chougan, M., Ghaffar, S.H., Nematollahi, B., Sikora, P., Dorn, T., Stephan, D., et al., 2022. Effect of natural and calcined halloysite clay minerals as low-cost additives on the performance of 3D-printed alkali-activated materials. Mater. Des. 223, 111183 https://doi.org/10.1016/j.matdes.2022.111183.

Cui, K., Chang, J., Feo, L., Chow, C.L., Lau, D., 2022. Developments and applications of carbon nanotube reinforced cement-based composites as functional building materials. Front. in Mater. 9, 861646 https://doi.org/10.3389/fmats.2022.861646.

Dulaj, A., Suijs, M.P.M., Salet, T.A.M., Lucas, S.S., 2022. Incorporation and characterization of multi-walled carbon nanotube concrete composites for 3D printing applications. In: Buswell, R., Blanco, A., Cavalaro, S., Kinnell, P. (Eds.), Third RILEM Int. Conf. On Concr. and Dig. Fab. DC 2022, vol. 37. RILEM Bookseries, Cham. https://doi.org/10.1007/978-3-031-06116-5_18. Springer.

Fang, Y., Li, L.Y., Dassekpo, J.B.M., Jang, S.H., 2021. Heat transfer modelling of carbon nanotube reinforced composites. Composites, Part B 109280. https://doi.org/10.1016/j.compositesb.2021.109280.

Jo, J.H., Jo, B.W., Cho, W., Kim, J.H., 2020. Development of a 3D printer for concrete structures: laboratory testing of cementitious materials. Int. J. of Concr. Struct. and Mater. 14 (1), 1–11. https://doi.org/10.1186/s40069-019-0388-2.

Kan, D., Liu, G., Cao, S.C., Chen, Z., Lyu, Q., 2022. Mechanical properties and pore structure of multiwalled carbon nanotube-reinforced reactive powder concrete for three-dimensional printing manufactured by material extrusion. 3D Print. Addit. Manuf. https://doi.org/10.1089/3dp.2022.0243.

Kazemian, A., Yuan, X., Cochran, E., Khoshnevis, B., 2017. Cementitious materials for construction-scale 3D printing: laboratory testing of fresh printing mixture. Construct. Build. Mater. 145, 639–647. https://doi.org/10.1016/j.conbuildmat.2017.04.015.

Khan, S.A., Ghazi, S.M.U., Amjad, H., Imran, M., Khushnood, R.A., 2024. Emerging horizons in 3D printed cement-based materials with nanomaterial integration: a review. Construct. Build. Mater. 411, 134815 https://doi.org/10.1016/j.conbuildmat.2023.134815.

Li, Z., Li, L.Y., 2022. Analysis of electrical conductivity of carbon nanotube-reinforced two-phase composites. Compos. Commun. 35, 101305 https://doi.org/10.1016/j.coco.2022.101305.

Ma, G., Li, Z., Wang, L., 2018. Printable properties of cementitious material containing copper tailings for extrusion based 3D printing. Construct. Build. Mater. 162, 613–627. https://doi.org/10.1016/j.conbuildmat.2017.12.051.

Muthukrishnan, S., Ramakrishnan, S., Sanjayan, J., 2021. Technologies for improving buildability in 3D concrete printing. Cem. Concr. Compos. 122, 104144 https://doi.org/10.1016/j.cemconcomp.2021.104144.

Panda, B., Shakor, P., Laghi, V., 2023. Additive Manufacturing for Construction.

Paolini, A., Kollmannsberger, S., Rank, E., 2019. Additive manufacturing in construction: a review on processes, applications, and digital planning methods. Addit. Manuf. 30, 100894 https://doi.org/10.1016/j.addma.2019.100894.

Pasupathy, K., Ramakrishnan, S., Sanjayan, J., 2022. Enhancing the properties of foam concrete 3D printing using porous aggregates. Cem. Concr. Compos. 133, 104687 https://doi.org/10.1016/j.cemconcomp.2022.104687.

Puzatova, A., Shakor, P., Laghi, V., Dmitrieva, M., 2023. Large-scale 3D printing for construction application by means of robotic arm and Gantry 3D Printer: a Review. Build 12. https://doi.org/10.3390/buildings12112023.

Ramezani, M., Dehghani, A., Sherif, M.M., 2022. Carbon nanotube reinforced cementitious composites: a comprehensive review. Construct. Build. Mater. 315, 125100 https://doi.org/10.1016/j.conbuildmat.2021.125100.

Rubio, M., Sonebi, M., Amziane, S., 2017. 3D printing of fibre cement-based materials: fresh and rheological performances, Acad. J. Civ. Eng. 35 (2), 480–488. https://doi.org/10.26168/icbbm2017.74.

Sanjayan, J.G., Nematollahi, B., Xia, M., Marchment, T., 2018. Effect of surface moisture on inter-layer strength of 3D printed concrete. Construct. Build. Mater. 172, 468–475. https://doi.org/10.1016/j.conbuildmat.2018.03.232.

Shakor, P., Nejadi, S., Paul, G., 2019. A study into the effect of different nozzles shapes and fibre-reinforcement in 3D printed mortar. Materials 12 (10), 1708. https://doi.org/10.3390/ma12101708.

Shakor, P., Nejadi, S., Gowripalan, N., 2020. Effect of heat curing and E6-glass fibre reinforcement addition on powder-based 3DP cement mortar. In: Second RILEM Int. Conf. On Concr. and Dig. Fabr.: Dig. Concr, vol. 2. Springer Int. Publishing, pp. 508–515. https://doi.org/10.1007/978-3-030-49916-7_52.

Sheikh, T.M., Anwar, M.P., Muthoosamy, K., Jaganathan, J., Chan, A., Mohamed, A.A., 2021. The mechanics of carbon-based nanomaterials as cement reinforcement—a critical review. Construct. Build. Mater. 303, 124441 https://doi.org/10.1016/j.conbuildmat.2021.124441.

Sikora, P., Chougan, M., Cuevas, K., Liebscher, M., Mechtcherine, V., Ghaffar, S.H., et al., 2021. The effects of nano-and micro-sized additives on 3D printable cementitious and alkali-activated composites: a review. Appl. Nanosci. 1–19. https://doi.org/10.1007/s13204-021-01738-2.

Sun, X., Wang, Q., Wang, H., Chen, L., 2020. Influence of multi-walled nanotubes on the fresh and hardened properties of a 3D printing PVA mortar ink. Construct. Build. Mater. 247, 118590 https://doi.org/10.1016/j.conbuildmat.2020.118590.

Wang, L., Aslani, F., 2023. Structural performance of reinforced concrete beams with 3D printed cement-based sensor embedded and self-sensing cementitious composites. Eng. Struct. 275, 115266 https://doi.org/10.1016/j.engstruct.2022.115266.

Wu, P., Wang, J., Wang, X., 2016. A critical review of the use of 3-D printing in the construction industry, Autom. Constr. Met. (CTICM) 68, 21–31. https://doi.org/10.1016/j.autcon.2016.04.005.

Yazdanbakhsh, A., Grasley, Z., Tyson, B., Al-Rub, R.A., 2012. Challenges and benefits of utilizing carbon nanofilaments in cementitious materials. J. Nanomater. 1–8. https://doi.org/10.1155/2012/371927.

Zhang, P., Su, J., Guo, J., Hu, S., 2023. Influence of carbon nanotube on properties of concrete: a review. Construct. Build. Mater. 369, 130388 https://doi.org/10.1016/j.conbuildmat.2023.130388.